Article

Synthesis of CoFe$_2$O$_4$/Peanut Shell Powder Composites and the Associated Magnetic Solid Phase Extraction of Phenoxy Carboxylic Acid Herbicides in Water

Dongliang Ji [ID], Zhaoqin Huang * and Buyun Du

College of Environment and Ecology, Jiangsu Open University, Nanjing 210036, China; jidl@jsou.edu.cn (D.J.); duby@jsou.edu.cn (B.D.)
* Correspondence: huangzq@jsou.edu.cn

Abstract: The magnetic biochar material CoFe$_2$O$_4$/PCPS (peanut shell powder) was prepared based on the hybrid calcination method. The properties of prepared composites and the extraction effect of magnetic solid phase extraction on phenoxy carboxylic acid herbicides were assessed. The morphology, crystal structure, specific surface area, and pore size distribution of the material were analysed using a transmission electron microscope (TEM), infrared Fourier transform infrared spectroscopy (FTIR), X-ray powder diffraction (XRD), X-ray photoelectron spectroscopy (XPS), and N$_2$ absorption surface analysis (BET). The results of the magnetic solid phase extraction of a variety of phenoxy carboxylic acid herbicides in water using CoFe$_2$O$_4$/PCPS composites showed that, when the mass ratio of CoFe$_2$O$_4$ and PCPS was 1:1, 40 mg of the composite was used, and the adsorption time was 10 min at pH 8.50. Methanol was used as the eluent, and the recovery rates of the three phenoxy carboxylic acid herbicides were maintained at 81.95–99.07%. Furthermore, the actual water sample analysis results showed that the established method had good accuracy, stability, and reliability.

Keywords: magnetic biochar material; phenoxy carboxylic acid herbicides; magnetic solid phase extraction; actual water sample

1. Introduction

Phenoxy carboxylic acid herbicides are widely used due to their low cost, effectiveness in weed control, and high water solubility [1,2]. However, they still have the potential to cause harm to animal and human populations, even though their concentrations in environmental water samples are relatively low. Long-term exposure will increase the risks of leukemia and non-Hodgkin lymphoma in children, endocrine disorders in organisms, and metabolic imbalance [3–6]. Therefore, it is of theoretical and practical significance to develop a method for detecting trace amounts of phenoxy carboxylic acid herbicides.

As a new technology for sample pretreatment, magnetic solid phase extraction (MSPE) can fully contact the target analyte and quickly enrich the analyte. The magnetic sorbents can be directly recycled by a magnet [7]. Consequently, MSPE has a high separation efficiency and convenient operation [8]. The key to the MSPE is the choice of sorbent. Generally, graphene oxide (GO), metal–organic frameworks (MOFs), covalent organic frameworks (COFs), carbon nanotubes (CNTs), and biochar (BC) may be used as sorbents. Biochar with a large specific surface area enables the efficient extraction of the target analyte from water [9]. In this work, the preparation of CoFe$_2$O$_4$/PCPS (peanut shell powder) and its physicochemical properties have been characterized. The magnetic biochar material CoFe$_2$O$_4$/PCPS was synthesized with peanut shell as the carbon source and CoFe$_2$O$_4$ as the magnetic nucleus. The CoFe$_2$O$_4$ had a face-centered cube structure formed by Fe^{3+}, Co^{2+}, and O^{2-}. Three substances, including 4-chlorophenoxyacetic acid, 2,4-dichlorophenoxyacetic acid, and 2,4-droplet propionic acid, were chosen as the target analytes, then the effects of preparation conditions and external factors on the recovery of analytes were

Int. J. Environ. Res. Public Health **2022**, *19*, 8450

2 of 12

discussed. Finally, a pretreatment method to concentrate the phenoxy carboxylic acid herbicides and their subsequent analysis was established.

2. Materials and Methods

2.1. Preparation of $CoFe_2O_4$ Nanoparticles

A total of 0.01 mol $Co(NO_3)_2 \cdot 6H_2O$ and 0.02 mol $FeCl_3 \cdot 6H_2O$ were added to beakers with 30 mL pure water. The pH was adjusted to 12 using a 30% NaOH solution. The mixture was stirred and sonicated for 1 h. Subsequently, the mixture was transferred to a vacuum drying oven and reacted at 120 °C for 10 h. The product was washed, dried, and stored for subsequent use.

2.2. Preparation of $CoFe_2O_4$/PCPS Composites

The fresh peanut shells were washed and oven-dried at 110 °C for 24 h, crushed into powder by a grinder, and then sieved. Particles with a diameter of 0.25–0.425 mm were collected. $CoFe_2O_4$ (1.0000 g), peanut shell powder (PCPS, 1.0000 g), and KCl (2.0000 g) were placed in a mortar and ground evenly. After this, the $CoFe_2O_4$, peanut shell powder (PCPS), and KCl mixture was stirred with 20 mL water for 24 h and oven dried at 120 °C for 12 h. Subsequently, the material was placed into a tube furnace with an argon atmosphere and calcined at 600 °C for 3 h. Finally, the sample was cleaned, dried, and named CS1 for subsequent use. Similarly, the materials with mass ratios of $CoFe_2O_4$ and PCPS of 1:0.5, 1:1.5, and 1:2 were named CS0.5, CS1.5, and CS2, respectively.

2.3. Collection of Environmental Water

Three river water samples were randomly gathered from the Yellow and Yangtze Rivers in addition to water samples from the Xuanwu Lake in Nanjing. The snow water was taken from the school campus. All the water samples were stored in the dark at low temperature. The samples were cleaned preliminarily through filtration using a 0.45 μm membrane.

2.4. Magnetic Solid Phase Extraction Experiment

A total of 40 mg magnetic nanocomposite was added into a 100 mL water sample and treated with ultrasonic waves for 10 min so that the mixture attained equilibrium of adsorption and desorption. Under the action of an external magnetic field, the water sample and the composite material were separated. Subsequently, 2 mL methanol was used to elute the analyte absorbed by the composite material. The eluent was analysed, and the analyte was detected by high performance liquid chromatography (HPLC). The material synthesis and MSPE process are shown in Figure 1. HPLC instrument configuration and chromatographic conditions are shown in Table 1. The standard curve is shown in Table 2.

Table 1. The HPLC instrument configuration and chromatographic conditions.

Item	Parameter
Instruments	Waters 2489
Detector	An UV/Visible detector
Chromatographic column	A Lichrospher C18 column (150 mm × 4.6 mm, 5 μm)
Detection wavelength	230 nm
Mobile phase (volume ratio)	Methanol to water to acetic acid = 50:50:0.2
Flow rate	$1.0 \text{ mL} \cdot \text{min}^{-1}$
Injection volume	20.0 μL
Column temperature	30 °C

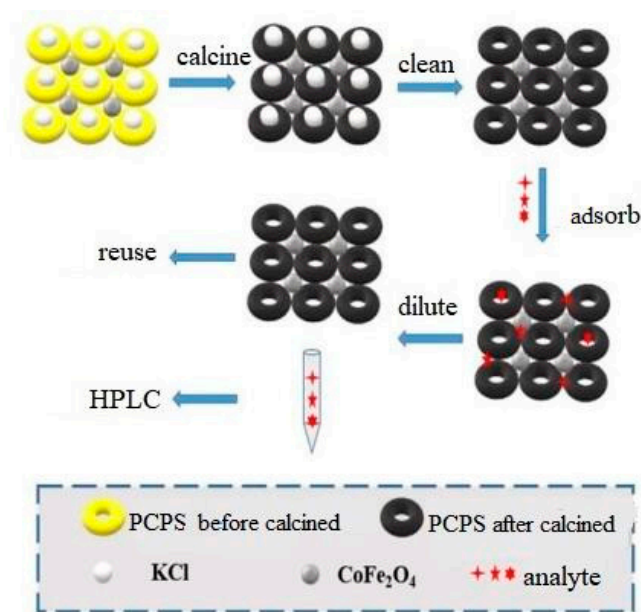*Int. J. Environ. Res. Public Health* **2022**, *19*, 8450

3 of 12

Figure 1. The schematic diagram of material synthesis and MSPE.

Table 2. Analytical parameters of MSPE-HPLC-UV method for the determination of phenoxy carboxylic acid pesticides in standard solution.

Analyte	Standard Curve	Linear Range ($\mu g \cdot L^{-1}$)	Correlation Coefficient (r^2)	LOD ($\mu g \cdot L^{-1}$)	LOQ ($\mu g \cdot L^{-1}$)
4-PA	$y = 60.4608x + 240.4391$	1.0–1000	0.9996	0.30	0.98
2,4-D	$y = 37.6800x + 984.8045$	2.0–1000	0.9978	0.58	1.94
2,4-DP	$y = 35.9193x - 832.7198$	2.0–1000	0.9995	0.59	1.96

2.5. Analysis Methods

A transmission electron microscope (TEM) (JEM-200 CX, JEOL, Tokyo, Japan) and scanning electron microscopy (SEM) (S-3400N II, Hitachi, Tokyo, Japan) were used to examine the morphological and chemical properties for the $CoFe_2O_4$/PCPS. A spectrometer (Tensor 27, Bruck, Germany) was used to obtain the infrared Fourier transform spectroscopy (FTIR) spectra of the $CoFe_2O_4$/PCPS. The samples were also analysed using X-ray photoelectron spectroscopy (XPS) (PHI 5000 Versa Probe, Ulvac-Phi, Chigasaki, Japan) and X-ray powder diffraction (XRD) (XRD-6000, Shimadzu, Tokyo, Japan). N_2 absorption surface analysis was used to characterize the specific surface area and pore size distribution (ASAP2050, Micromertics, Norcross, GA, USA). Chromatographic analysis was recorded on a Waters HPLC (Waters 2489, Waters, Milford, MA, USA).

2.6. The Determination of Zete Potential

The samples were added to 50 mL purified water at a solid–liquid ratio of 1:1. After ultrasonic dispersion, the pH of the system was adjusted with 0.1 $mol \cdot L^{-1}$ HCL and NaOH. The potential of supernatant was determined by Zeta potentiometer. Each sample was measured three times.

3. Results

3.1. Morphology Analysis

The material surface morphologies are shown in Figure 2, in which Figure 2A–C displays the transmission electron microscope (TEM), high-resolution transmission electron microscopy (HRTEM), and selected area electron diffraction (SAED) images of $CoFe_2O_4$,

Int. J. Environ. Res. Public Health **2022**, *19*, 8450

4 of 12

respectively. Figure 2F displays the TEM and HRTEM images of PCPS. Finally, Figure 2G–I shows the TEM, HRTEM, and SAED images of $CoFe_2O_4$/PCPS, respectively.
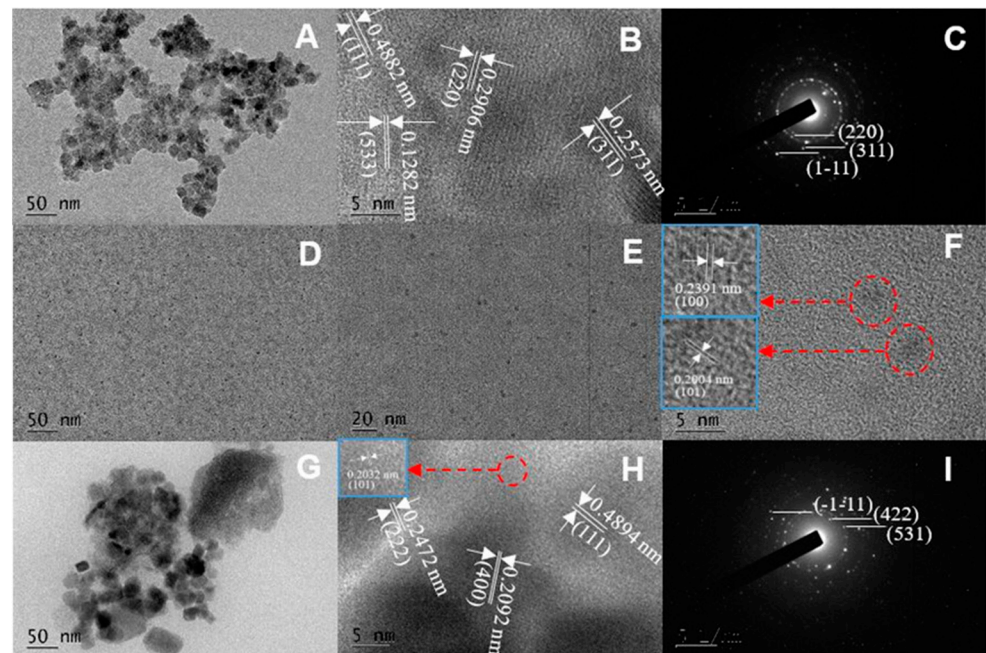

Figure 2. The TEM, HRTEM, and SAED images of $CoFe_2O_4$ (**A–C**); the TEM images of PCPS (**D,E**) and HRTEM (**F**); the TEM, HRTEM, and SAED images of $CoFe_2O_4$/PCPS (**G–I**).

As shown in Figure 2A–C, the $CoFe_2O_4$ was composed of homogeneous nanoparticles with diameters of 10–20 nm. The lattice planes with separation distances of 0.4882, 0.2906, 0.2573, and 0.1282 nm corresponded to the (111), (220), (311), and (533) $CoFe_2O_4$ lattice planes, respectively [10,11]. Figure 2D,E exhibited the presence of carbon quantum dots that were distributed uniformly within the size interval of 1.3–2.5 nm. Two groups of lattice fringes in Figure 2F represented the crystal planes (100) and (101) for graphite carbon [12–14]. Figure 2G exhibited that many holes were distributed on the PCPS lamellar structure. The $CoFe_2O_4$ lattice-stripe nanoparticles appeared in Figure 2H,I. This indicated that $CoFe_2O_4$ nanoparticles had been successfully compounded with PCPS.

3.2. XRD Analysis

Figure 3A–C represents the typical XRD pattern for PCPS, $CoFe_2O_4$, and $CoFe_2O_4$/PCPS XRD, respectively.
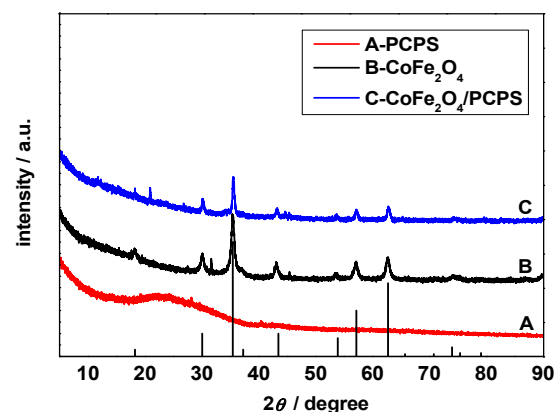

Figure 3. XRD patterns of synthesized PCPS (**A**), $CoFe_2O_4$ (**B**), and $CoFe_2O_4$/PCPS (**C**).

Figure 3A shows broad peaks at 24.0°, which were indexed as the (002) graphite carbon planes [15–19]. Nine discernible diffraction peaks are observed in Figure 3B, including those at 18.2°, 30.1°, 35.5°, 43.5°, 53.9°, 57.2°, 62.7°, 65.7°, and 74.0°. They can be ascribed to the (111), (220), (311), (400), (422), (511), (440), (531), and (533) planes, respectively [20]. Figure 3C shows that the diffraction peaks of $CoFe_2O_4$ were diminished due to the covering PCPS; however, the crystal shape did not change.

3.3. FTIR Analysis

The infrared spectra of $CoFe_2O_4$ (A), PCPS (B), and $CoFe_2O_4$/PCPS (C) are shown in Figure 4.

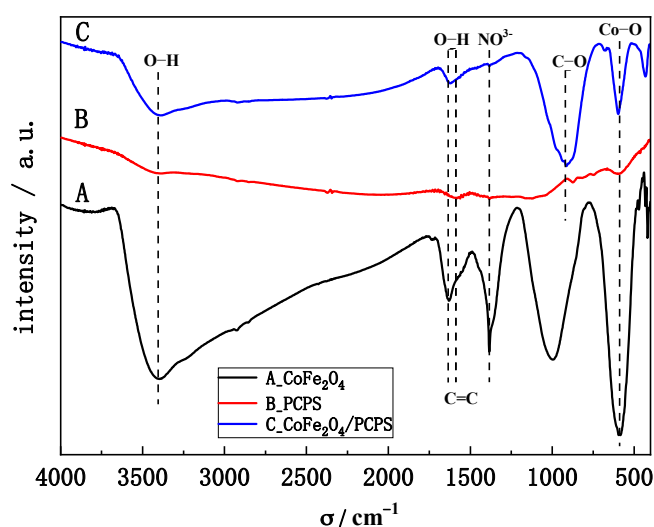**Figure 4.** FTIR spectra for synthesized $CoFe_2O_4$ (**A**), PCPS (**B**), and $CoFe_2O_4$/PCPS (**C**).

The band at approximately 3405 cm^{-1} represented the O-H stretching vibration [21] and is shown in Figure 4A–C. The bands at 1635 cm^{-1}, 1384 cm^{-1}, and 400–650 cm^{-1} were assigned to the O-H, NO^{3-}, Fe-O, and Co-O groups [22], respectively. These bands are shown in Figure 4A. The bands at 1588 cm^{-1}, 1379 cm^{-1}, and 980–1200 cm^{-1} were attributed to the C=C, -COOH, C-O, and OH groups [23,24], respectively. As shown in Figure 4C, all the generally observed peaks for $CoFe_2O_4$ and PCPS were present in the synthesized materials, but their spectrum intensities decreased slightly. All the results indicate that the composite possessed oxygen-containing and carbon-containing functional groups on the surface. These groups can adsorb target molecules by hydrophobic interaction and hydrogen bonding [25].

3.4. XPS Analysis

Figure 5 shows the XPS spectra in the prepared $CoFe_2O_4$/PCPS composite. The spectra for C, O, Fe, and Co along with their chemical bonding states are shown in Figure 5A–D, respectively. The illustration shown in Figure 5A displays the full spectrum of these elements.

As shown in Figure 5A, the C 1 s, O 1s, Fe 2p, and Co 2p binding energies were 285.9 eV, 529.4 eV, 714.0 eV, and 782.8 eV, respectively. The atomic ratio for Co and Fe was 1:2, which corresponds with the atom number ratio of Co and Fe in $CoFe_2O_4$. The binding energies 284.5 eV, 284.8 eV, 286.1 eV, and 288.8 eV were attributed to the C=C, C-H, C-O, and (C=O)OH functional groups. The binding energies of 530.3 eV, 531.0 eV, 532.0 eV, and 533.2 eV in Figure 5B were attributed to lattice oxygen, Fe-O-C, C(O)OH, and C-OH, respectively. In addition, the binding energies shown in Figure 5C,D—712.1 eV, 725.8 eV, 781.2 eV, and 782.6 eV—were attributed to the Fe 2p3/2 and Fe 2p1/2 octahedron along with the Co^{2+} tetrahedron, respectively [26,27].
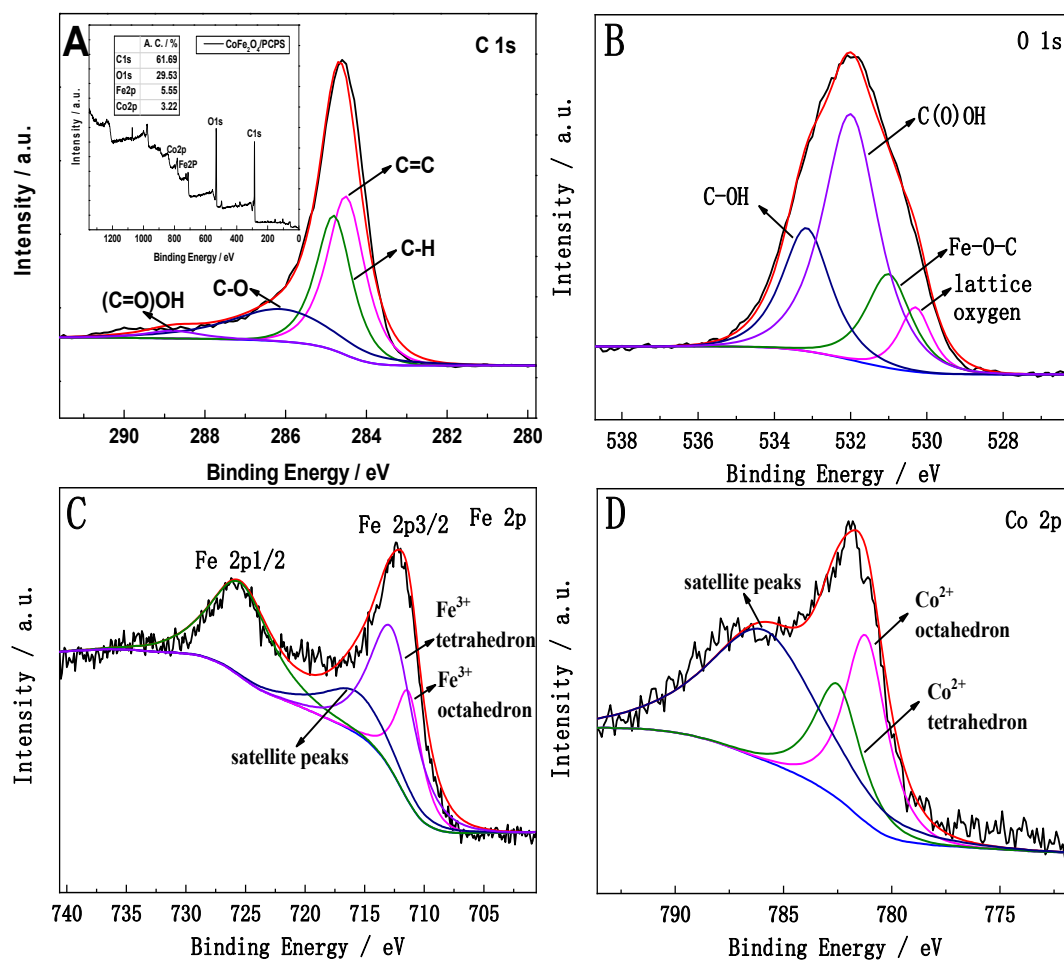
Figure 5. XPS for $CoFe_2O_4$/PCPS: full scan spectra [the inset in (**A**)], C 1s spectra (**A**), O 1s spectra (**B**), Fe 2p spectra (**C**), and Co 2p spectra (**D**).

3.5. N_2 Adsorption-Desorption Analysis

　　Figure 6A–C represents the nitrogen adsorption–desorption curves for $CoFe_2O_4$, PCPS and $CoFe_2O_4$/PCPS, respectively. The illustrations in each figure displayed their pore size distribution, which was also shown in the figure panels.

　　As shown in Figure 6, the N_2 adsorption–desorption isotherms for $CoFe_2O_4$ conformed to type III, while the PCPS isotherms and the $CoFe_2O_4$/PCPS conformed to type IV. The pore sizes of $CoFe_2O_4$, PCPS, and $CoFe_2O_4$/PCPS were 9.7–20.3 nm, 0.6–2.0 nm, and 1.8–20.5 nm, respectively. This indicated that $CoFe_2O_4$/PCPS was microporous and mesoporous materials. In addition, the specific surface areas of $CoFe_2O_4$, PCPS, and $CoFe_2O_4$/PCPS were 4.64, 152.90, and 146.03 $m^2 \cdot g^{-1}$, respectively, which indicated that PCPS still had a large specific surface area after covering $CoFe_2O_4$.
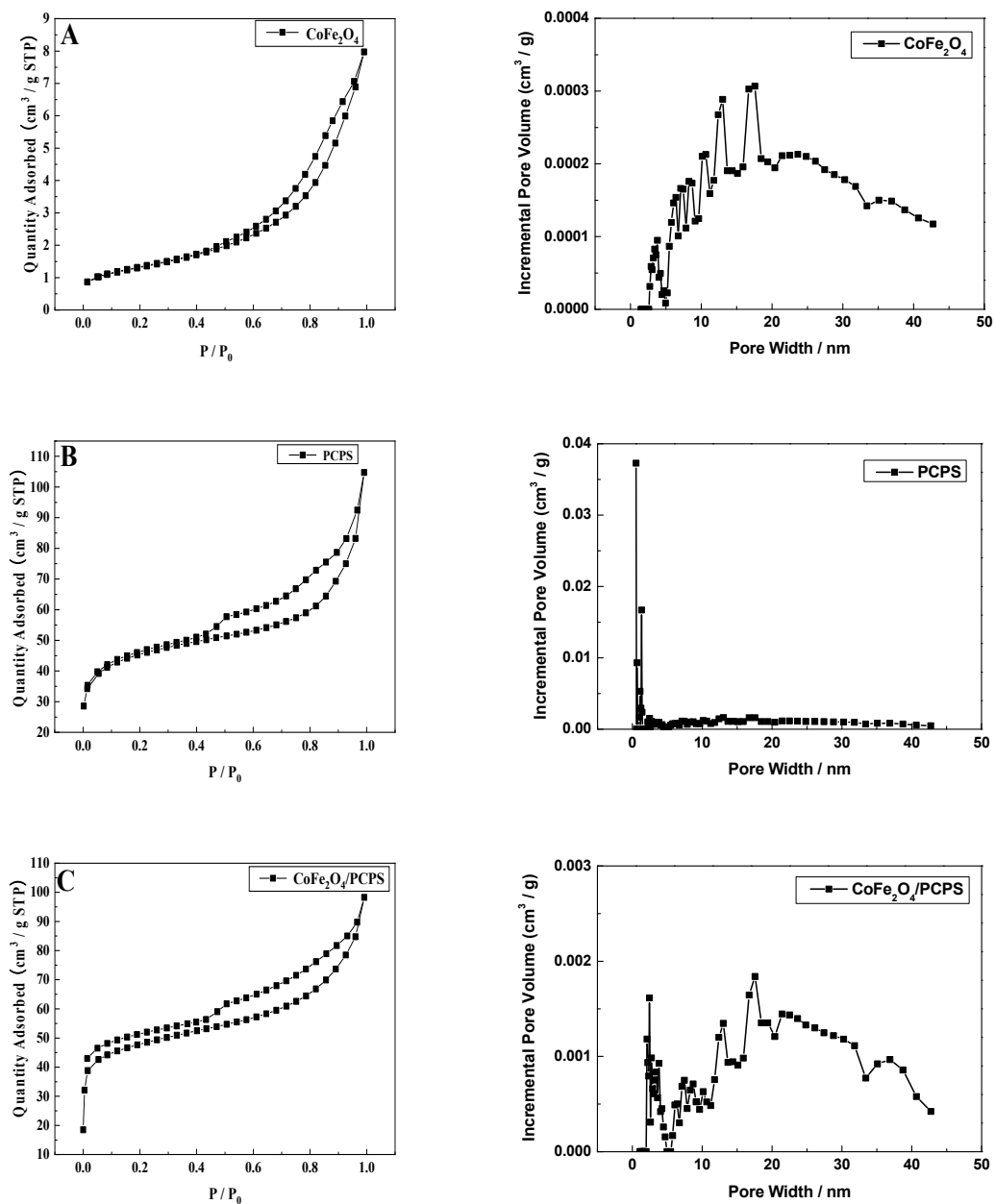
Figure 6. N_2 adsorption–desorption isotherms and the pore size distribution of the $CoFe_2O_4$ (**A**), PCPS (**B**), and $CoFe_2O_4$/PCPS (**C**).

3.6. MSPE Condition Optimizing

3.6.1. Material Components

Magnetic solid phase extraction was performed using the prepared materials to discuss the influence of material components on extraction effects. For each treatment, 40 mg CS0.5, CS1, CS1.5, and CS2 composite materials were added into four samples containing 100 mL analyte (4-PA, 2,4-D, 2,4-DP) at concentrations of $0.04\ mg \cdot L^{-1}$ each. Subsequently, they were eluted by 2 mL acetonitrile. The results were shown in Figure 7.

Int. J. Environ. Res. Public Health **2022**, *19*, 8450

8 of 12

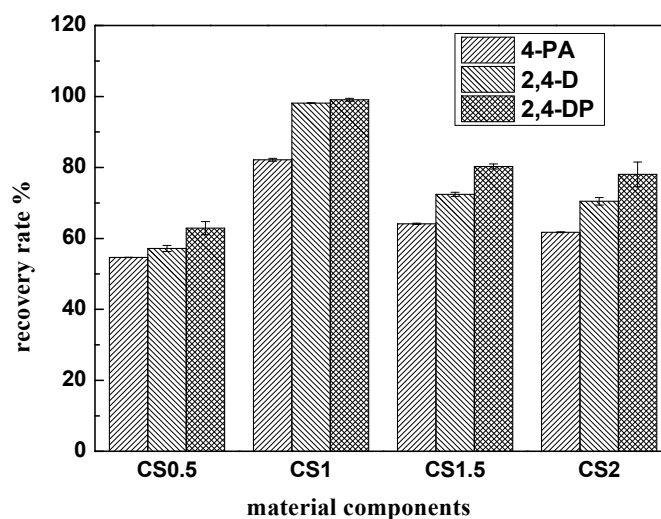**Figure 7.** The effect of material composition on the magnetic solid phase extraction.

As shown in Figure 7, the CS1 composite possessed the best magnetic solid phase extraction effect for three analytes. The principal reason was that when the carbon content was lower, the material had fewer adsorption sites. This was not conducive to adsorption of the analyte on the material surface, resulting in a relatively low recovery rate. When the carbon content increased, the magnetic properties of the composite diminished, and the composites were difficult to separate from the water sample under external magnetic fields. Therefore, the CS1 material with a $CoFe_2O_4$ and PCPS mass ratio of 1:1 was selected in the following experiments.

3.6.2. Conditional Experiment

The effects of composite dosage, pH, eluent type, adsorption time, and enrichment factor on the pretreatment of the target analyte in the magnetic solid phase extraction process are shown in Figure 8.

Figure 8A shows that the recovery rates of the analytes increased with increasing dosages of CS1. When the SC1 dosage reached 40 mg, the recovery rate of the analytes exceeded 82.17%, but as the usage of CS1 continued to increase, the recoveries of the three analytes remained between 81.17% and 99.77%. However, the elution process in the subsequent treatment became more difficult. Therefore, 40 mg should be selected as the appropriate dosage. From the results of Figure 8B, we found that the target analyte had the optimum recovery at a pH of 8.50. A possible cause is that the surface of the material was negatively charged in the weakly alkaline system (Figure 8C). The carboxylate ions dissociated from the target pollutants may have combined with the material through the electrostatic effect of NH_4^+ in the buffer solution; this is beneficial to the adsorption process. As Figure 8D shows, the magnetic solid phase extraction effect was optimal when methanol was used as the eluent and the recovery rate of phenoxy carboxylic acid herbicides was between 82.17 and 99.07%. Consequently, methanol was used as the eluent in the magnetic solid phase extraction experiment.

The speed of magnetic solid phase extraction determined the viability of this method for practical application. As shown in Figure 8E, the recoveries of the three phenoxy carboxylic herbicides increased initially and subsequently stabilized. When the adsorption time was less than eight minutes, the recoveries of the analytes were less than 55.72%. When the adsorption time was greater than ten minutes, the recovery rate was between 81.95% and 99.07%. Equilibrium between adsorption and desorption was observed. The enrichment factor condition experiment from Figure 8F showed that when the enrichment factor was greater than 75, the recovery rates of the three phenoxy carboxylic herbicides were all less than 80%. This was because increasing the sample volume reduced the mass of material contained per sample volume; consequently, the analyte could not be completely

Int. J. Environ. Res. Public Health **2022**, *19*, 8450

9 of 12

adsorbed. Therefore, 50 was determined as the enrichment factor in the magnetic solid phase extraction experiment. According to Figure 8G, the recovery of SC1 does not decrease significantly after 10 recycles.
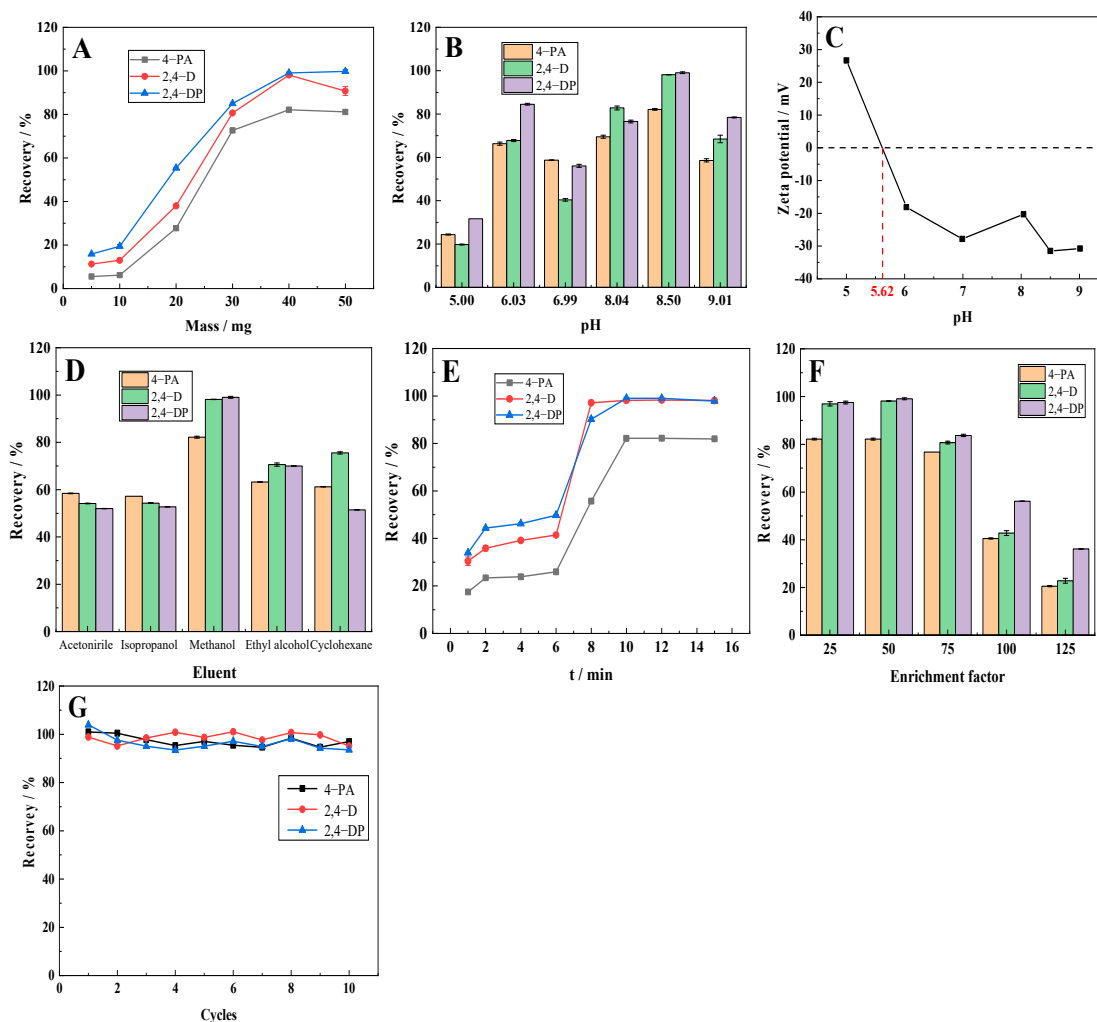

Figure 8. The effect of dosage (**A**), pH (**B**), Zeta potential (**C**), eluent type (**D**), adsorption time (**E**), enrichment factor (**F**), and cycles (**G**) on three phenoxy carboxylic acid herbicides.

3.7. Analysis of Environmental Water Samples

To verify the reliability of the established method, the MSPE method was used to analyse actual water samples from the Yellow and Yangtze Rivers, Xuanwu Lake, and snow melt. None of the collected water samples were contaminated by 4-PA, 2,4-D, or 2,4-DP. The water samples were spiked with 0.02 mg·L^{-1} and 0.04 mg·L^{-1} of each analyte. Based on magnetic solid phase extraction and high-performance liquid chromatography, the analyte recoveries varied from 75.22% to 94.66%, and the relative standard deviation (RSD) ranged from 0.08% to 3.70%, as shown in Table 3. Comparing the method established in this paper with other reported methods, as shown in Table 4 [1,28–31], the results of the current study showed that the pretreatment method based on CoFe$_2$O$_4$/PCPS magnetic biochar material had good accuracy, stability, and reliability.

Table 3. The recovery and RSD of the three analytes in real water samples (na = 3).

Water Samples	Standard Addition Concentration (mg·L^{-1})	Detection of Concentration (mg·L^{-1})			Recovery Rate [b]/% (*RSD*/%)		
		4-PA	2,4-D	2,4-DP	4-PA	2,4-D	2,4-DP
Yellow River	0	——	——	——			
	0.02	0.0164	0.0175	0.0189	81.75 (1.66)	87.45 (2.06)	94.66 (3.15)
	0.04	0.0333	0.0346	0.0355	83.27 (2.39)	86.41 (1.52)	88.63 (1.99)
Xuanwu Lake	0	——	——	——			
	0.02	0.0150	0.0159	0.0177	75.22 (1.25)	79.66 (3.35)	88.29 (3.70)
	0.04	0.0335	0.0333	0.0347	83.82 (0.85)	83.13 (3.15)	86.70 (2.97)
Yangtze River	0	——	——	——			
	0.02	0.0161	0.0163	0.0163	80.27 (0.61)	81.65 (1.89)	81.50 (1.25)
	0.04	0.0336	0.0353	0.0370	84.04 (2.27)	88.15 (1.62)	92.61 (0.08)
Snow melt	0	——	——	——			
	0.02	0.0155	0.0161	0.0162	77.30 (1.48)	80.36 (1.38)	81.08 (0.56)
	0.04	0.0328	0.0339	0.0358	81.88 (2.62)	84.86 (1.73)	89.54 (1.46)

Detection times; [b]: average value of three parallel experiments.

Table 4. Method comparison.

Method	Analytical Sample	Sample Volume /mL	Pre-Conditioning Time/min	LODs (µg·L^{-1})			*RSD*/%	Recovery Rate/%	Reference
				4-PA	2,4-D	2,4-DP			
DSPE [a]	tap water and lake water	50	13		0.2–0.3		1.4–8.6	83.7–114.4	[1]
SPE	river water and waste water	750	11			0.3–6.3	1.1–11.4	95–104	[28]
SPE	distilled water, stream and well water	200	100		0.02		0.2–4.0	80.0–110.0	[29]
SPE	river water	400	90		0.01			50.0–80.0	[30]
µ-SPE [b]-MSPE	Reservoir raw water	10	45		0.2		1.7–5.1	89.0–103.0	[31]
MSPE	river water, lake water and snow water	100	10	0.3	0.58	0.59	0.08–3.70	75.22–94.66	this text

[a]: Dispersed solid phase extraction; [b]: micro solid phase extraction.

4. Conclusions

In this paper, a CoFe$_2$O$_4$/PCPS composite was prepared via the biopyrolysis method and applied to the magnetic solid phase extraction of three phenoxy carboxylic herbicides (4-PA, 2,4-D, 2,4-DP) dissolved in water. The influence of material composition, dosage, pH, adsorption time, eluent, enrichment factor, and cycles on the magnetic solid phase extraction effect was discussed. The optimal conditions were applied for the actual detection of the herbicides in environmental water samples, and the main conclusions were as follows:

(1) The characterizations such as TEM, XRD, FTIR, and BET demonstrated that the CoFe$_2$O$_4$/PCPS composite was successfully synthesized. The material maintained the original structure of PCPS and had a large specific surface area and pore volume.

(2) In the optimization experiment of magnetic solid phase extraction conditions, phenoxy carboxylic herbicides were extracted using 40 mg of the composite material, and adsorption occurred in water samples with a pH of 8.50 for 10 min. The best magnetic solid phase extraction effect was obtained with methanol as the eluent. The

Int. J. Environ. Res. Public Health **2022**, *19*, 8450

11 of 12

recovery rates of all the analyte were greater 82.17%. The material still maintains high performance after ten cycles.

(3)   When the established method was applied to environmental water samples, the recoveries were 75.22–94.66%. The RSD was 0.08–3.70%.

Author Contributions: Conceptualization, D.J.; methodology, D.J., Z.H. and B.D.; software, B.D.; validation, D.J., Z.H. and B.D.; formal analysis, B.D.; investigation, D.J.; resources, D.J., Z.H. and B.D.; data curation, Z.H.; writing—original draft preparation, D.J.; writing—review and editing, Z.H.; visualization, B.D. and Z.H.; supervision, D.J.; project administration, Z.H.; funding acquisition, D.J. All authors have read and agreed to the published version of the manuscript.

Institutional Review Board Statement: Not applicable.

Informed Consent Statement: Not applicable.

Data Availability Statement: Not applicable.

Conflicts of Interest: The authors declare no conflict of interest.

References

1.   Wang, J.; Zhu, J.; Si, L.; Du, Q.; Li, H.; Bi, W.; da Young Chen, D. High throughput screening of phenoxy carboxylic acids with dispersive solid phase extraction followed by direct analysis in real time mass spectrometry. *Anal. Chim. Acta* **2017**, *996*, 20–28. [CrossRef] [PubMed]

2.   Yuan, X.; Liu, C.; Zhao, J.; Zhao, P.; Zhao, L. A novel magnetic multi-walled carbon nanotube-based magnetic solid-phase extraction combined with dispersive liquid-liquid microextraction method for the determination of four phenoxy carboxylic acid herbicides in food crops by using ultra-high performance liquid chromatography-tandem mass spectrometry. *Anal. Methods* **2018**, *10*, 3263–3272.

3.   Malagoli, C.; Costanzini, S.; Heck, J.E.; Malavolti, M.; De Girolamo, G.; Oleari, P.; Palazzi, G.; Teggi, S.; Vinceti, M. Passive exposure to agricultural pesticides and risk of childhood leukemia in an Italian community. *Int. J. Hyg. Environ. Health* **2016**, *219*, 742–748. [CrossRef] [PubMed]

4.   de Arcaute, C.R.; Soloneski, S.; Larramendy, M.L. Toxic and genotoxic effects of the 2,4-dichlorophenoxyacetic acid (2,4-D)-based herbicide on the Neotropical fish *Cnesterodon decemmaculatus*. *Ecotoxicol. Environ. Saf.* **2016**, *128*, 222–229. [CrossRef] [PubMed]

5.   Wang, F.; Zhang, W.; Chen, Y.; Xu, G.; Deng, Z.; Du, H.; Wang, Y.; Zhang, S.; Zhao, W. Simultaneous determination of six plant growth regulators in fruits using high performance liquid chromatography based on solid-phase extraction and cleanup with a novel mixedmode functionalized calixarene sorbent. *Anal. Methods* **2015**, *7*, 6365–6371. [CrossRef]

6.   Manna, S.; Saha, P.; Roy, D.; Sen, R.; Adhikari, B. Removal of 2,4-dichlorophenoxyacetic acid from aqueous medium using modified jute. *J. Taiwan Inst. Chem. Eng.* **2016**, *67*, 292–299. [CrossRef]

7.   Liao, Y.; Huang, X.; Wang, Z.; Gan, R. Progress in application of magnetic solid phase extraction in detection and analysis. *Food Sci.* **2011**, *32*, 317–320. (In Chinese)

8.   Xu, Y.; Jin, J.; Li, X.; Han, Y.; Meng, H.; Wu, J.; Zhang, X. Rapid magnetic solid-phase extraction of Congo Red and Basic Red 2 from aqueous solution by ZIF-8@CoFe$_2$O$_4$ hybrid composites. *J. Sep. Sci.* **2016**, *39*, 3647–3654. [CrossRef]

9.   Wang, L.; Wang, J.; Wang, Z.; He, C.; Lyu, W.; Yan, W.; Yang, L. Enhanced antimonate (Sb(V)) removal from aqueous solution by La-doped magnetic biochars. *Chem. Eng. J.* **2018**, *354*, 623–632. [CrossRef]

10.   Köseoğlu, Y. Rapid Synthesis of Nanocrystalline NiFe$_2$O$_4$ and CoFe$_2$O$_4$ Powders by a Microwave-Assisted Combustion Method. *J. Supercond. Nov. Magn.* **2013**, *26*, 1391–1396. [CrossRef]

11.   Ji, G.B.; Tang, S.L.; Ren, S.K. Simplified synthesis of single-crystalline magnetic CoFe$_2$O$_4$ nanorods by a surfactant-assisted hydrothermal process. *J. Cryst. Growth* **2004**, *270*, 156–161. [CrossRef]

12.   Martindale, B.C.; Hutton, G.A.; Caputo, C.A.; Reisner, E. Solar hydrogen production using carbon quantum dots and a molecular nickel catalyst. *J. Am. Chem. Soc.* **2015**, *137*, 6018–6025. [CrossRef] [PubMed]

13.   Zhang, Y.L.; Hu, L.L.; Sun, Y. One-step synthesis of chiral carbon quantum dots and their enantioselective recognition. *RSC Adv.* **2016**, *6*, 59956–59960. [CrossRef]

14.   Kauser, A. Polymer/carbon-based quantum dot nanocomposite: Forthcoming materials for technical application. *J. Macromlecular Sci. Part A* **2019**, *56*, 341–356. [CrossRef]

15.   Zhou, H.; Wu, S.; Wang, H.; Li, Y.; Liu, X.; Zhou, Y. The preparation of porous carbon materials derived from bio-protic ionic liquid with application in flexible solid-state supercapacitors. *J. Hazard. Mater.* **2021**, *402*, 124023. [CrossRef]

16.   De Andres, P.L.; Ramírez, R.; Vergés, J.A. Strong covalent bonding between two graphene layers. *Phys. Rev. B* **2008**, *77*, 0745403. [CrossRef]

Int. J. Environ. Res. Public Health **2022**, *19*, 8450

12 of 12

17. Liang, H.X.; Song, B.; Peng, P. Preparation of three-dimensional honeycomb carbon materials and their adsorption of Cr(VI). *Chem. Eng. J.* **2019**, *367*, 9–16. [CrossRef]

18. Yuan, D.S.; Chen, J.X.; Zeng, J.H.; Tan, S.X. Preparation of monodisperse carbon nanospheres for electrochemical capacitors. *Electrochem. Commun.* **2008**, *10*, 1067–1070. [CrossRef]

19. Wu, Y.; Hu, S.H.; Xu, R.; Wang, J.W. Boosting Potassium-Ion Battery Performance by Encapsulating Red Phosphorus in Free-Standing Nitrogen-Doped Porous Hollow Carbon Nanofibers. *Nano Lett.* **2019**, *19*, 1351–1358. [CrossRef]

20. Wu, Q.; Zhang, H.; Zhou, L.; Bao, C.; Zhu, H.; Zhang, Y. Synthesis and application of rGO/CoFe$_2$O$_4$ composite for catalytic degradation of methylene blue on heterogeneous Fenton-like oxidation. *J. Taiwan Inst. Chem. Eng.* **2016**, *67*, 484–494. [CrossRef]

21. Limaye, M.V.; Singh, S.B.; Das, R.; Poddar, P.; Abyaneh, M.K.; Kulkarni, S.K. Magnetic studies of SiO$_2$ coated CoFe$_2$O$_4$ nanoparticles. *J. Magn. Magn. Mater.* **2017**, *441*, 683–690. [CrossRef]

22. Wu, X.; Wang, W.; Li, F.; Khaimanov, S.; Tsidaeva, N.; Lahoubi, M. PEG-assisted hydrothermal synthesis of CoFe$_2$O$_4$ nanoparticles with enhanced selective adsorption properties for different dyes. *Appl. Surf. Sci.* **2016**, *389*, 1003–1011. [CrossRef]

23. Yang, J.; Qiao, J.Q.; Cui, S.H.; Li, J.Y.; Zhu, J.J.; Yin, H.X.; Zhan, C.Y.; Lian, H.Z. Magnetic solid-phase extraction of brominated flame retardants from environmental waters with graphene-doped Fe$_3$O$_4$ nanocomposites. *J. Sep. Sci.* **2015**, *38*, 1969–1976. [CrossRef] [PubMed]

24. Banerjee, M.; Bar, N.; Basu, R.K.; Das, S.K. Comparative study of adsorptive removal of Cr(VI) ion from aqueous solution in fixed bed column by peanut shell and almond shell using empirical models and ANN. *Environ. Sci. Pollut. Res.* **2017**, *24*, 10604–10620. [CrossRef]

25. Geng, X.; Lv, S.; Yang, J.; Cui, S.; Zhao, Z. Carboxyl-functionalized biochar derived from walnut shells with enhanced aqueous adsorption of sulfonamide antibiotics. *J. Environ. Manag.* **2021**, *280*, 111749. [CrossRef]

26. Tang, X.Q.; Zhang, Y.D.; Jiang, Z.W.; Wang, D.M.; Huang, C.Z.; Li, Y.F. Fe$_3$O$_4$ and metal-organic framework MIL-101(Fe) composites catalyze luminol chemiluminescence for sensitively sensing hydrogen peroxide and glucose. *Talanta* **2018**, *179*, 43–50. [CrossRef]

27. Wang, W.P.; Yang, H.; Xian, T.; Jiang, J.L. XPS and magnetic properties of CoFe$_2$O$_4$ nanoparticles synthesized by a polyacrylamide gel route. *Mater. Trans.* **2012**, *53*, 1586–1589. [CrossRef]

28. Valimaña-Traverso, J.; Morante-Zarcero, S.; Pérez-Quintanilla, D.; García, M.Á.; Sierra, I.; Marina, M.L. Cationic amine-bridged periodic mesoporous organosilica materialsfor off-line solid-phase extraction of phenoxy acid herbicides fromwater samples prior to their simultaneous enantiomeric determination by capillary electrophoresis. *J. Chromatogr. A* **2018**, *1566*, 146–157. [CrossRef]

29. Thorstensen, C.W.; Lode, O.; Christiansen, A.L. Development of a solid-phase extraction method for phenoxy acids and bentazone in water and comparison to a liquid-liquid extraction method. *J. Agric. Food Chem.* **2000**, *48*, 5829–5833. [CrossRef]

30. Loos, R.; Locoro, G.; Contini, S. Occurrence of polar organic contaminants in the dissolved water phase of the Danube River and its major tributaries using SPE-LC-MS2 analysis. *Water Res.* **2010**, *44*, 2325–2335. [CrossRef]

31. Dong, S.Y.; Huang, G.Q.; Su, M.L.; Huang, T. Environmentally friendly method: Development and application to carbon aerogel as sorbent for solid-phase extraction. *ACS Appl. Mater. Interfaces* **2015**, *7*, 22256–22263. [CrossRef] [PubMed]